PHYSICAL REVIEW B VOLUME 39, NUMBER 1 1 JANUARY 1989

Energy transfer between Er^{3+} and Tm^{3+} ions in a barium fluoride–thorium fluoride glass

D. C. Yeh, R. R. Petrin, and W. A. Sibley
Department of Physics, Oklahoma State University, Stillwater, Oklahoma 74078-0444

V. Madigou and J. L. Adam
Laboratoire de Chimie Minerale D, Université de Rennes-Beaulieu, 35042 Rennes Cédex, France

M. J. Suscavage
Solid State Sciences Directorate, Rome Air Development Center, Hanscom Air Force Base, Bedford, Massachusetts 01731
(Received 6 June 1988; revised manuscript received 6 September 1988)

The up-conversion of infrared radiation into green, red, and 805-nm fluorescence has been studied for Er^{3+} and Tm^{3+} ions in both Yb^{3+}-doped and non-Yb^{3+}-doped BaF_2-ThF_4 fluoride glass over a wide temperature range and several dopant concentrations. It has been found that the addition of Tm^{3+} preferentially quenches the up-conversion efficiency of the green emission corresponding to a transition from the $^4S_{3/2}$ level of Er^{3+}. The decrease in emission amounts to a factor of about 50 for a concentration of 0.5 mol % TmF_3 at 300 K. The quenching effect is discussed in terms of energy transfer between Er^{3+} and Tm^{3+} ions. A rate equation model and a Judd-Ofelt analysis used in conjunction with the appropriate optical data lead to an understanding of the up-conversion process. The absolute values of the energy transfer rates and the electron populations in the lower excited states of the excited Er^{3+} and Tm^{3+} ions can be determined. This information should enable researchers to tailor materials to improve the efficiency of the up-conversion and laser devices.

I. INTRODUCTION

The passive conversion of infrared light to visible light, frequency up-conversion, has been extensively studied in rare-earth-doped materials by many investigators.[1–3] This process could play an important role in enhancing optical detection and display devices. In addition, the advent of near-infrared semiconductor diode lasers has made possible up-conversion pumping of rare-earth laser systems.[4–8] The recent developments in heavy-metal fluoride glasses have been very helpful in this area.[9–11] Only recently a Nd^{3+}-doped heavy-metal fluoride glass fiber laser was reported.[12]

The development of an efficient fiber laser compatible with fluoride fiber systems would be beneficial for optical communication. However, for maximum efficiency, complicated multidoped systems must be used. For example, relatively high up-conversion efficiencies, through energy transfer, have been reported for BaF_2-ThF_4 heavy-metal fluoride glass co-doped with Yb^{3+}-Er^{3+} and Yb^{3+}-Tm^{3+} ion combinations.[13–15] On the other hand, van der Ziel *et al.* have reported that the addition of Tm^{3+} to an Er^{3+}-doped YF_3 crystal preferentially quenches the emission from the higher-energy Er^{3+} levels when a 1.5-μm pump radiation source is used.[16] They attributed this to energy transfer between Er^{3+} and Tm^{3+} ions and, in fact, energy transfer between Er^{3+} and Tm^{3+} ions in CdF_2 crystals have been extensively studied by Jouart.[17]

In this paper, the up-conversion processes for Er^{3+} and Tm^{3+} ions in both Yb^{3+}-doped and non-Yb^{3+}-doped BaF_2-ThF_4 fluoride glasses are investigated. It is necessary to determine experimentally and theoretically how to enhance both up-conversion and laser efficiencies. The kinetics of the up-conversion processes can be described by using rate equation models[2,6,8,13,14,16,18] in which the up-conversion fluorescence intensity is expressed in terms of transition probabilities, fluorescence lifetimes, and energy transfer rates.[2] A combination of experimental data, rate equations, and a Judd-Ofelt analysis[13,14,19–27] of absorption data to determine transition probabilities allows energy transfer rates to be found. This approach can be used to predict impurity types and concentrations which will provide more efficient up-conversion glass systems through the filling and depletion of various levels.

II. EXPERIMENTAL PROCEDURE

The samples used for this investigation were prepared at the Rome Air Development Center, Hanscom Air Force Base, and Laboratoire de Chimie Minerale D, Université de Rennes, France. Details of the preparative techniques have been described earlier.[28–30] The compositions of these glasses are listed in Table I. The digits (I) or (II) following the compositional acronym indicate samples with different concentrations of TmF_3 and YbF_3.

Low-temperature measurements were performed in a CTI Model 21 SC Cryodyne Cryocooler with a resistance heater which allowed temperature control within ± 1 K over the range 15–300 K. The absorption spectra were carried out on a Perkin-Elmer model 330 spectrophotometer. Integrated intensities were determined by numerical integration.

Emission spectra were obtained by exciting the samples with a light from a 150-W xenon-arc lamp passed through a Spex Spectramate model 1680B double mono-

TABLE I. Compositions of glasses (mol %).

Glass	BaF_2	ZnF_2	InF_3	YF_3	YbF_3	LuF_3	ThF_4	ErF_3	TmF_3
A(I) [BZIYbTETm(I)]	30	20	30		8.5		10	1	0.5
A(II) [BZIYbTETm(II)]	30	20	28.9		10		10	1	0.1
B (BZIYTETm)	28.63	18.63	28.64	10			10	4	0.1
C (BZLTE)	19	27				23	27	4	
D (BZYbTLE)	19	27			5	21	27	1	
E (BZYbTTm)	19	27			26		27		1
F (BZYbTLTm)	19	27			26	0.95	27		0.05

chromator. The fluorescence was focused into a 0.8-m Spex monochromator and a mirror was used to route the light emerging from the exit slit to the appropriate detector. The detectors were a cooled RCA C31034 photomultiplier tube (PMT), for the visible, and an Optoelectronics OTC-22-53 PbS cell, for the infrared. The signal from the detector was preamplifier and passed to a lock-in amplifier whose reference was a variable-speed light chopper in the excitation beam. The output of the look-in amplifier was displayed on an X-Y recorder or stored in a Hewlett-Packard HP-86B minicomputer. The intensity of the exciting light at the sample position was measured with a model PR200 pyroelectric radiometer. The excited area of the sample was 0.054 cm^2. The excitation spectra have been corrected for wavelength dependence of the system. The emission spectra have been corrected based on the calibration of the optical system with a quartz-iodine standard lamp traceable to the National Bureau of Standards.

Lifetime measurements were performed by storing the preamplifier signal in a Nicolet model 1070 signal averager. For fast lifetimes the preamplifier signal was sent to a Biomation 610B transient recorder and stored in the Nicolet signal averager. This system allowed lifetimes as short as 10 μs to be measured.

III. EXPERIMENTAL RESULTS

The absorption spectrum of glass A(I) at 80 K is shown in Fig. 1. The symbols E, T, and Y represent lines due to Er^{3+}, Tm^{3+}, and Yb^{3+}, respectively. The band positions and intensities for Er^{3+} and Tm^{3+} are in agreement with earlier measurements on BaF_2-ThF_4 fluoride glass.[13,14] The absorption spectra are similar for all the samples used in this study and the absorption coefficients are proportional to the concentrations of Er^{3+}, Tm^{3+}, and Yb^{3+} ions in the samples.

A Judd-Ofelt analysis has been employed to determine the radiative transition probabilities and the branching ratios for Er^{3+} and Tm^{3+} transitions in BaF_2-ThF_4 fluoride glass. Details of the theory and method have been well described earlier;[13,19–27] hence, only the results will be presented here. The matrix elements $U^{(t)}$, used in the present work, were calculated by Weber[22] for Er^{3+} in LaF_3 and by Carnall, Crosswhite, and Crosswhite[31] for Tm^{3+} in LaF_3. The matrix elements are almost host invariant.[24,25] The values of measured and calculated oscillator strengths (f) for various transitions for 2 mol % ErF_3 and 2 mol % TmF_3 in BaF_2-ThF_4 fluoride glasses at room temperature are shown in Tables II and III, respectively. The Judd-Ofelt parameters Ω_t were determined from a least-squares fit to the values of measured oscillator strengths. These were found to be $\Omega_2=2.19\times10^{-20}$ cm^2, $\Omega_4=1.52\times10^{-20}$ cm^2, and $\Omega_6=9.12\times10^{-21}$ cm^2 for the 2-mol % ErF_3 sample. The rms deviation of f calculated from the residuals is 1.85×10^{-7}. For the 2-mol % TmF_3 sample, the Judd-Ofelt parameters are $\Omega_2=2.02\times10^{-20}$ cm^2, $\Omega_4=1.56\times10^{-20}$ cm^2, and $\Omega_6=1.10\times10^{-20}$ cm^2. The rms deviation of f is 10^{-7}. The rms deviations from the both Er^{3+} and Tm^{3+} samples are comparable to the rms deviations found by applying the Judd-Ofelt theory to other rare-earth ions in fluoride glass systems.[13,14,25–27] The values of A_{ED}, A_{MD}, τ_R and the branching ratio for Er^{3+} and Tm^{3+} samples are listed in Tables IV and V, respectively. The quantities A_{ED} and A_{MD} are the electric and magnetic dipole transition probabilities and τ_R is the radiative lifetime.

Figure 2 shows the emission spectrum of glass A(I) excited at 356 nm within the $^2G_{7/2}$ level of Er^{3+} and $^1D_2$ level of Tm^{3+} at room temperature. The excitation spectra were measured for the emission lines shown in the figure. Based on these spectra and the energies of the J manifold obtained by absorption measurements, the fluorescent transitions were assigned. In the figure the asterisk labels the transition $^1D_2\rightarrow{}^3H_4$, the plus indicates

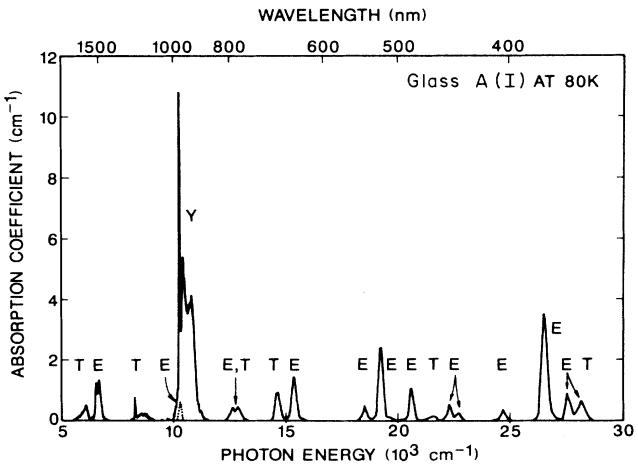

FIG. 1. Absorption spectra of Er^{3+}, Tm^{3+}, and Yb^{3+} in glass A(I) at 80 K.

TABLE II. Measured and calculated oscillator strengths of Er^{3+} in BaF_2-ThF_4 fluoride glass at 300 K. All transitions are from the $^4I_{15/2}$ level to the level indicated.

Level	Wavelength (nm)	Average frequency (cm^{-1})	10^{-8} oscillator strength Measured	Calculated	10^{-8} residual
$^4I_{11/2}$	977.2	10233	38.28	29.24	9.04
$^4I_{9/2}$	802.4	12463	19.05	19.15	−0.10
$^4F_{9/2}$	653.4	15305	139.20	133.29	5.91
$^4S_{3/2}$	542.6	18430	35.54	26.06	9.48
$^2H_{11/2}$	520.9	19198	254.54	293.05	−38.51
$^4F_{7/2}$	488.1	20488	103.37	110.52	−7.15
$^4F_{5/2}$	449.3	22257	31.90	30.81	1.09
$^4F_{3/2}$	441.8	22635	22.80	16.86	5.94
$^2H_{9/2}$	405.9	24637	33.30	45.73	−12.43
$^4G_{11/2}$	378.4	26427	545.16	523.75	21.41

TABLE III. Measured and calculated oscillator strengths of Tm^{3+} in BaF_2-ThF_4 fluoride glass at 300 K. All transitions are from the $^3H_6$ level to the level indicated.

Level	Wavelength (nm)	Average frequency (cm^{-1})	10^{-8} oscillator strength Measured	Calculated	10^{-8} residual
$^3H_4$	1709.4	5850	119.46	121.68	−2.22
$^3F_4$	785.9	12724	137.27	137.81	−0.54
$^3F_3, ^3F_2$	685.3	14592	213.65	207.57	6.08
$^1G_4$	468.4	21349	47.17	39.48	7.69
$^1D_2$	356.7	28035	141.48	145.01	−3.53
$^1I_6, ^3P_0$	286.5	34904	57.71	55.20	2.51
$^3P_1$	274.8	36390	21.65	41.52	−19.87
$^3P_2$	261.8	38197	139.54	139.70	−0.16

TABLE IV. Predicted spontaneous-emission probabilities of Er^{3+} in BaF_2-ThF_4 fluoride glass.

Transition	Average frequency (cm^{-1})	A_{ED} (sec^{-1})	A_{MD} (sec^{-1})	τ_R (msec)	Branching ratios
$^4I_{13/2} \rightarrow ^4I_{15/2}$	6410	64.6	33.3	10.2	1.00
$^4I_{11/2} \rightarrow ^4I_{15/2}$	10040	78.9		10.2	0.80
$\rightarrow ^4I_{13/2}$	3630	10.2	9.3		0.20
$^4I_{9/2} \rightarrow ^4I_{15/2}$	12262	93.3		8.18	0.76
$\rightarrow ^4I_{13/2}$	5852	26.4			0.22
$\rightarrow ^4I_{11/2}$	2222	0.6	1.9		0.02
$^4F_{9/2} \rightarrow ^4I_{15/2}$	14970	965.9		0.95	0.92
$\rightarrow ^4I_{13/2}$	8560	47.3			0.05
$\rightarrow ^4I_{11/2}$	4930	34.7			0.03
$\rightarrow ^4I_{9/2}$	2708	1.0			
$^4S_{3/2} \rightarrow ^4I_{15/2}$	18083	696.7		0.96	0.67
$\rightarrow ^4I_{13/2}$	11673	280.8			0.27
$\rightarrow ^4I_{11/2}$	8043	22.4			0.02
$\rightarrow ^4I_{9/2}$	5821	37.5			0.04
$^2H_{11/2} \rightarrow ^4I_{15/2}$	18904	2870.4		0.35	1.00
$^2H_{9/2} \rightarrow ^4I_{15/2}$	24390	917.5		0.46	0.42
$\rightarrow ^4I_{13/2}$	17980	942.1			0.43
$\rightarrow ^4I_{11/2}$	14350	280			0.13
$\rightarrow ^4I_{9/2}$	12128	10.6			0.01
$\rightarrow ^4F_{9/2}$	9420	22.5			0.01

TABLE V. Predicted spontaneous-emission probabilities of Tm^{3+} in BaF_2-ThF_4 fluoride glass.

Transition	Average frequency (cm^{-1})	A_{ED} (sec^{-1})	A_{MD} (sec^{-1})	τ_R (msec)	Branching ratios
$^3H_4 \rightarrow {}^3H_6$	5365	94.3		10.6	1.00
$^3H_5 \rightarrow {}^3H_6$	7892	126.7	44.6	5.66	0.97
$\rightarrow {}^3H_4$	2428	4.0	1.3		0.03
$^3F_4 \rightarrow {}^3H_6$	12469	622.3		1.45	0.90
$\rightarrow {}^3H_4$	6725	51.9			0.08
$\rightarrow {}^3H_5$	4098	13.2			0.02
$^3F_3 \rightarrow {}^3H_6$	14184	1295.0		0.68	0.88
$\rightarrow {}^3H_4$	8726	40.3			0.03
$\rightarrow {}^3H_5$	6101	129.8			0.09
$\rightarrow {}^3F_4$	1880	2.2	0.6		
$^3F_2 \rightarrow {}^3H_6$	14727	401.7		1.23	0.49
$\rightarrow {}^3H_4$	9268	263.9			0.32
$\rightarrow {}^3H_5$	6644	142.2			0.18
$\rightarrow {}^3F_4$	2422	6.0			0.01
$\rightarrow {}^3F_3$	463	0.01	0.01		
$^1G_4 \rightarrow {}^3H_6$	20833	507.1		0.86	0.44
$\rightarrow {}^3H_4$	15267	96.4			0.08
$\rightarrow {}^3H_5$	12674	397.7			0.34
$\rightarrow {}^3F_4$	8460	118.2			0.10
$\rightarrow {}^3F_3$	6575	35.4			0.03
$\rightarrow {}^3F_2$	6035	10.2			0.01
$^1D_2 \rightarrow {}^3H_6$	27548	5815.0		0.07	0.40
$\rightarrow {}^3H_4$	22075	6520.1			0.45
$\rightarrow {}^3H_5$	19646	75.5			0.01
$\rightarrow {}^3F_4$	15221	832.9			0.06
$\rightarrow {}^3F_3$	13333	465.8			0.03
$\rightarrow {}^3F_2$	12937	575.1			0.04
$\rightarrow {}^1G_4$	6793	91.7			0.01

the transition $^4S_{3/2} \rightarrow {}^4I_{13/2}$, the circle defines the transition $^4F_{9/2} \rightarrow {}^4I_{13/2}$, the square denotes the transition $^4I_{11/2} \rightarrow {}^4I_{13/2}$, the triangle designates the combination of the transitions $^2H_{11/2} \rightarrow {}^4I_{15/2}$ and $^1D_2 \rightarrow {}^3H_5$, the double asterisk identifies the combination of the transitions $^4F_{9/2} \rightarrow {}^4I_{15/2}$, $^1G_4 \rightarrow {}^3H_4$, and $^1D_2 \rightarrow {}^3F_4$, the double circle marks the transitions $^1D_2 \rightarrow {}^3F_3$, the double square means the combination of the transitions $^1D_2 \rightarrow {}^3F_2$, $^1G_4 \rightarrow {}^3H_5$, and $^3F_4 \rightarrow {}^3H_6$, and the double plus indicates the combination of the transitions $^2F_{5/2} \rightarrow {}^2F_{7/2}$ and $^4I_{11/2} \rightarrow {}^4I_{15/2}$. All other transitions are from excited states to the ground state.

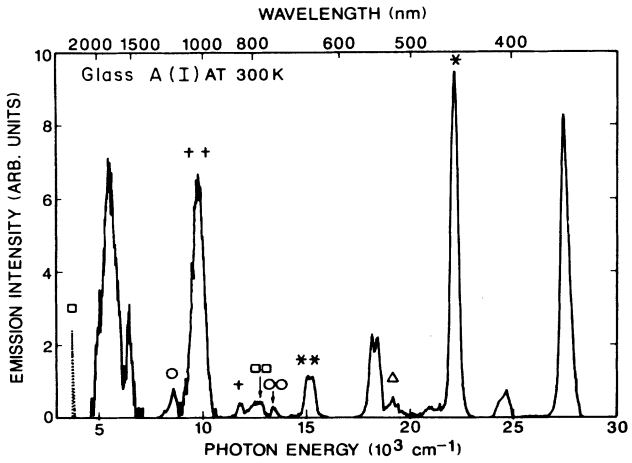

FIG. 2. Emission spectra of Er^{3+}, Tm^{3+}, and Yb^{3+} in glass A(I) at 300 K. The symbols above the bands are explained in the text. The relative intensities between the visible and the ir emission are arbitrary. Bands plotted as dotted lines have had their intensities increased by a factor of 10.

The 300-K excitation spectra of the Tm^{3+} $^3H_4$ emission for glasses E and A(I) are illustrated in Figs. 3(b) and 3(c). The room-temperature absorption spectrum of glass A(I) is shown in Fig. 3(a) for comparison. The symbols *E* and *T* denoted in this figure represent the Er^{3+} and Tm^{3+} absorption bands. Figure 3(d) presents the Er^{3+} $^4I_{13/2} \rightarrow {}^4I_{15/2}$ excitation spectrum for glass A(I). The *sharp* line of the Yb^{3+} absorption spectra at 973 nm appears as a broad band in the excitation spectra in Fig. 3 due to poor resolution of 12 nm for the excitation spectra. The Er^{3+} $^4F_{9/2}$ band appears in the Tm^{3+} excitation spectrum shown in Fig. 3(c), which indicates energy transfer from Er^{3+} to Tm^{3+} ions. Furthermore, the Tm^{3+} bands are also shown in Fig. 3(d), which suggests energy transfer from Tm^{3+} to Er^{3+} ions. The Yb^{3+} band (973 nm) appears in Figs. 3(b)–3(d), which indicates that Yb^{3+} ions transfer to both Er^{3+} and Tm^{3+} ions, since in Figs. 3(d) and 3(c) Tm^{3+} emission is detected and in Fig. 3(d) Er^{3+} emission is detected.

Figure 4(a) shows the room-temperature absorption spectrum of glass B in the range of 600–900 nm. The room-temperature excitation spectra of the Er^{3+}

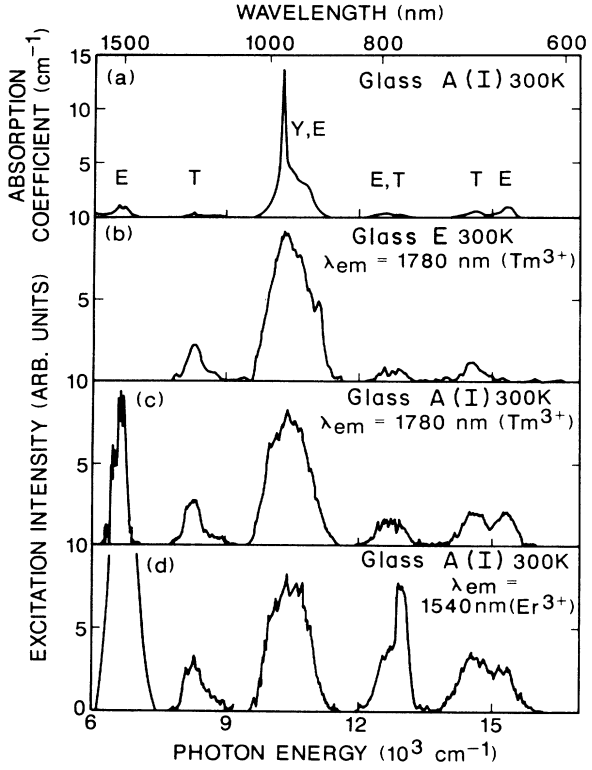

FIG. 3. (a) Absorption spectra of Er^{3+}, Tm^{3+}, and Yb^{3+} in glass A(I) at 300 K. Excitation spectra of the Tm^{3+} $^3H_4 \rightarrow {}^3H_6$ emission for (b) glass E and (c) glass A(I) at 300 K. (d) Excitation spectra of the Er^{3+} $^3I_{13/2} \rightarrow {}^4I_{15/2}$ emission for glass A(I) at 300 K.

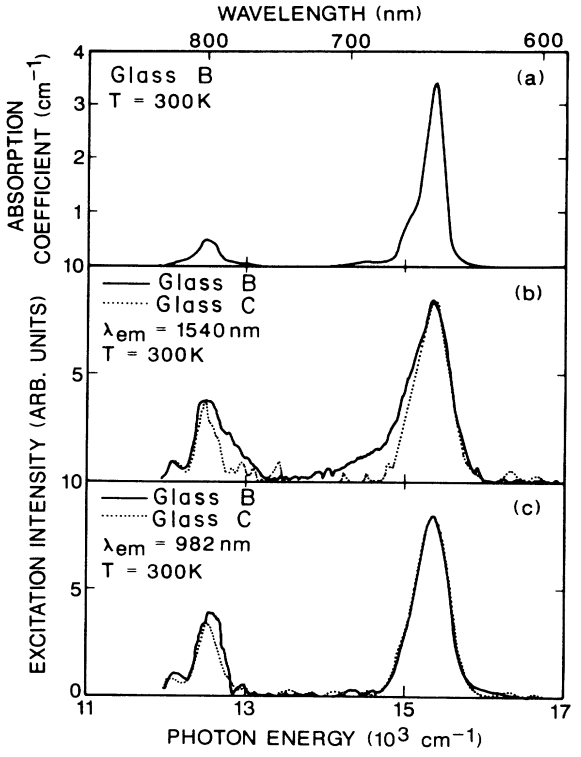

FIG. 4. (a) Absorption spectra of Er^{3+} and Tm^{3+} in glass B at 300 K. Excitation spectra of (b) Er^{3+} $^4I_{13/2} \rightarrow {}^4I_{15/2}$ emission and (c) Er^{3+} $^4I_{11/2} \rightarrow {}^4I_{15/2}$ emission for glass B (solid line) and glass C (dotted line) at 300 K.

$^4I_{13/2} \rightarrow {}^4I_{15/2}$ emission for glasses B and C are illustrated in Fig. 4(b) by solid and dashed lines, respectively. The excitation spectra for both samples with the transition monitored by the $^4I_{11/2} \rightarrow {}^4I_{15/2}$ transition are portrayed in Fig. 4(c). It is interesting to note that the Tm^{3+} $^3F_2$, $^3F_3$, and $^3F_4$ bands appear in Fig. 4(b) but not in Fig. 4(c). This suggests that the energy transfer from Tm^{3+} to Er^{3+} ions is due to the cross relaxation of the $^3F_4 \rightarrow {}^3H_4$ transition instead of the $^3F_4 \rightarrow {}^3H_6$ transition.

The temperature dependence of the $^4S_{3/2}$ and $^4F_{9/2}$ emission decay lifetimes for glass A(I), containing 1 mol % ErF_3 and 0.5 mol % TmF_3, and glass A(II), containing 1 mol % ErF_3 and 0.1 mol % TmF_3, is shown in Fig. 5. Also included in the figure for comparison are the previously reported data for glass D.[13] For these lifetime measurements the emission levels were *directly* excited. This procedure is especially important when slow nonradiative rates are involved. The error in these measurements is estimated to be ±5%. The decay for the transitions from these two levels was very nearly a single exponential. The first *e*-folding time was used as the value for the lifetime.

The up-conversion emission spectra for glass A(I) at 15 K, pumped with 973 nm light (bandwidth 8 nm) and measured in the range of 500–900 nm, are shown in Fig. 6. The energies of the emission spectra are consistent with

TABLE VI. Up-conversion efficiencies η for an incident absorbed light intensity of 16.5 mW/cm^2 for Yb^{3+}-doped BaF_2-ThF_4 fluoride glasses and of 9.3 mW/cm^2 for non-Yb^{3+}-doped BaF_2-ThF_4 fluoride glasses at 15 K as well as 6.5 mW/cm^2 at 300 K.

							$10^{-6}\eta$						
Emission	Glass A(I)			Glass A(II)			Glass C		Glass B		Glass D		Glass F
level (nm)	550	660	805	550	660	805	550	660	550	660	550	660	805
T (K)													
15	1.7	19	7.3	8.7	23		52	6.6	36	25	24	29	310
300	0.7	6.8	14	4.7	10	29	5.2	2	3.4	4.2	23	14	200

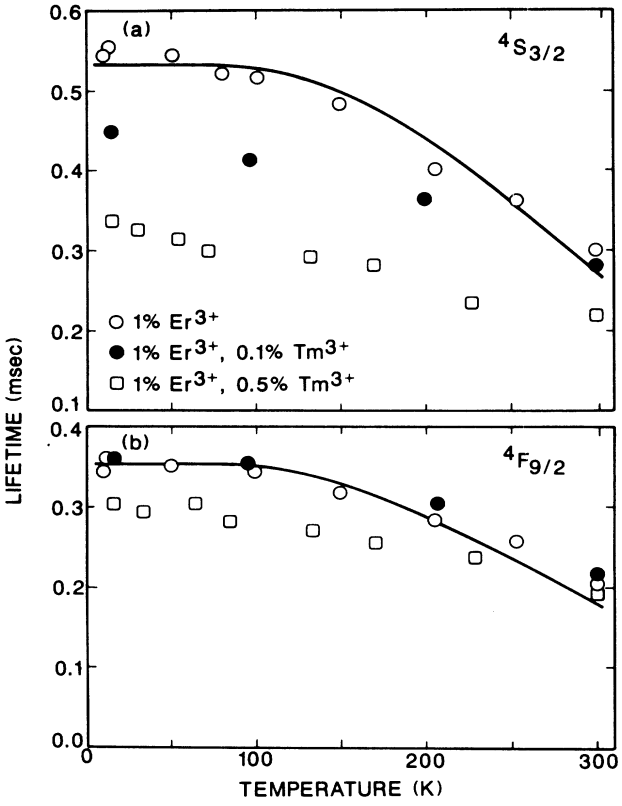

FIG. 5. Temperature dependence of the (a) $^4S_{3/2}$ and (b) $^4F_{9/2}$ emission lifetimes.

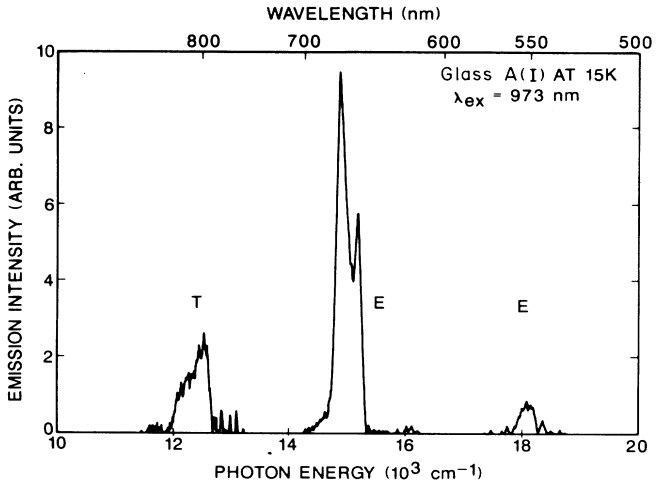

FIG. 6. Up-conversion emission spectra of glass A(I) at 15 K under 973-nm excitation. The symbols *E* and *T* represent lines due to Er^{3+} and Tm^{3+}, respectively.

those observed by direct excitation fluorescence from $^4S_{3/2}\rightarrow{}^4I_{15/2}$, $^4F_{9/2}\rightarrow{}^4I_{15/2}$, and $^3F_4\rightarrow{}^3H_6$. The symbols *E* and *T* indicated in this figure represent the Er^{3+} and Tm^{3+} emissions, respectively. There is a quadratic dependence of the fluorescence intensity for these transitions on the excitation intensity over the entire range of available pump power as observed previously.[13,14] These results indicate that the green ($^4S_{3/2}$), red ($^4F_{9/2}$), and near-ir ($^3F_4$) emitting states are predominantly populated by a two-photon absorption process.

The up-conversion efficiency is defined

$$\eta = I_{\text{out}}/I_{\text{abs}} , \tag{1}$$

where I_{out} is the emitted light intensity and I_{abs} the absorbed incident light intensity. The intensity of the absorbed light at the sample position was measured to be 16.5 mW/cm^2 in a band centered at 973 nm with 8-nm half-width for the samples doped with Yb^{3+} ions. For the non-Yb^{3+}-doped samples the pumping level was 970 nm, the peak position of $^4I_{11/2}$ absorption band of Er^{3+} ions, and the incident absorbed light intensity was 9.3 mW/cm^2 at 15 K and 6.4 mW/cm^2 at 300 K. Details of the technique used to determine I_{out} have been described previously.[13] The up-conversion efficiencies of $^4S_{3/2}$, $^4F_{9/2}$, and $^3F_4$ emissions for the sample used in this study are listed in Table VI. The previously reported up-conversion efficiencies of $^4S_{3/2}$ and $^4F_{9/2}$ emissions for glass D, containing 5 mol% YbF_3 and 1 mol% ErF_3, and of $^3F_4$ emission for glass F, containing 26 mol% YbF_3 and 0.05 mol% TmF_3, are included in this table for comparison.[13,14] The error in the absolute values can be 50%.

The up-conversion efficiency for $^4S_{3/2}$ emission in glass A(I) glass at 15 K is about 15 times smaller than that for glass D. However, the $^4F_{9/2}$ red up-conversion emission is only reduced by a factor of 2 at 15 K. As can be seen in Table VI, the addition of Tm^{3+} impurity ions preferentially quenches the up-conversion efficiency of the $^4S_{3/2}$ green emission, as observed previously by van der Ziel *et al.*[16] They used 1.5-μm infrared excitation of $Y_{1-x-y}Er_xTm_yF_3$ crystals. For the case of non-Yb^{3+}-doped fluoride glasses, the up-conversion efficiency for $^4S_{3/2}$ emission is reduced by a factor of about 2 with the addition of 0.1 mol% TmF_3 at 15 K. No Tm^{3+} $^3F_4$ up-conversion emission was detected from glass B at either 15 or 300 K.

IV. DISCUSSION

A. Judd-Ofelt analysis

A Judd-Ofelt analysis is necessary to evaluate up-conversion efficiency.[13,14] Jorgensen and Reisfeld noted that the Ω_2 parameter of the analysis is indicative of the amount of covalent bonding, while the Ω_6 parameter is related to the rigidity of the host.[32] The Ω_t intensity parameters for Er^{3+} and Tm^{3+} in various glasses are provided in Tables VII and VIII, respectively. The oxide glasses have large Ω_2 and small Ω_6 values, whereas fluoride glasses have comparable values for all three Ω_t's. The Ω_2 values for fluoride glasses are smaller than those for oxide glasses, which suggests that the fluoride glasses are more ionic in character.

TABLE VII. Ω_t parameters for Er^{3+} in various glasses. Numbers appearing before compounds in formulas represent mol % of constituent.

Glass	Ω_2 (10^{-20} cm^2)	Ω_4 (10^{-20} cm^3)	Ω_6 (10^{-20} cm^{-2})	Ref.
Borate	11.3	3.6	2.2	33
	15.3	4.2	2.5	34
Phosphate	9.32	3.51	1.28	35
	10.12	3.38	1.94	34
Germanate	7.45	1.22	0.54	35
	11.49	3.96	1.89	34
$57ZrF_4$-$34BaF_2$-$4AlF_3$-$3LaF_3$-$2ErF_3$	3.26	1.85	1.14	36
	2.54	1.39	0.97	26
$19BaF_2$-$27ZnF_2$-$5YbF_3$-$27ThF_4$-$21LuF_3$-$1ErF_3$	2.44	1.55	1.18	13
$30BaF_2$-$20ZnF_2$-$30InF_3$-$8YF_3$-$10ThF_4$-$2ErF_3$	2.19	1.52	0.91	This work

B. Energy transfer

Energy transfer between Yb^{3+}-Er^{3+} and Yb^{3+}-Tm^{3+} dopants has been extensively studied in crystals and glasses, and energy transfer between Er^{3+} and Tm^{3+} ions in YF_3 (Ref. 16) and CdF_2 (Ref. 17) crystals has been recently reported. The up-conversion efficiency of green, red, and 805-nm fluorescence for Er^{3+} and Tm^{3+} ions in Yb^{3+} doped BaF_2-ThF_4 fluoride glass, as shown in Table VI, is strongly influenced by energy transfer, and a knowledge of the energy transfer values between Er^{3+} and Tm^{3+} ions is essential.

As shown in Fig. 5(a), the $^4S_{3/2}$ lifetime decreases from 0.55 ms to 0.34 ms at 15 K and from 0.3 ms to 0.22 ms at room temperature with the addition of 0.5 mol % TmF_3. This indicates that energy transfer occurs from the Er^{3+} ions to the Tm^{3+} ions. The interaction of energy transfer between Er^{3+} and Tm^{3+} can be easily understood from the energy match for pairs of transitions as shown in the energy-level diagrams for Yb^{3+}, Er^{3+}, and Tm^{3+} in Fig. 7. The decrease in the $^4S_{3/2}$ lifetime due to the presence of Tm^{3+} is likely due to the resonant interactions

$$Er^{3+}: {}^4S_{3/2} \rightarrow {}^4I_{9/2}, \quad Tm^{3+}: {}^3H_6 \rightarrow {}^3H_4 ,$$

$$Er^{3+}: {}^4S_{3/2} \rightarrow {}^4I_{11/2}, \quad Tm^{3+}: {}^3H_6 \rightarrow {}^3H_5 .$$

In addition, the introduction of 0.5 mol % TmF_3 slightly quenches the $^4F_{9/2}$ lifetimes, as depicted in Fig. 5(b). This is due to the transitions

$$Er^{3+}: {}^4F_{9/2} \rightarrow {}^4I_{13/2}, \quad Tm^{3+}: {}^3H_6 \rightarrow {}^3H_5 ,$$

$$Er^{3+}: {}^4F_{9/2} \rightarrow {}^4I_{11/2}, \quad Tm^{3+}: {}^3H_6 \rightarrow {}^3H_4 ,$$

$$Er^{3+}: {}^4F_{9/2} \rightarrow {}^4I_{15/2}, \quad Tm^{3+}: {}^3H_6 \rightarrow {}^3F_2 .$$

In the first case, the Er^{3+}: $^4F_{9/2} \rightarrow {}^4I_{13/2}$ transition excites Tm^{3+} from the ground state to the $^3H_5$ level. The $^3H_5$ level then nonradiatively decays to the emitting $^3H_4$ level by multiphonon relaxation. This mechanism for the first two pairs of transitions is consistent with the observation of the $^4F_{9/2}$ band in the excitation spectrum of the Tm^{3+} $^3H_4 \rightarrow {}^3H_6$ emission band in glass A(I), as shown in Fig. 3(c). The strong $^4I_{13/2}$ band of Er^{3+} shown in this excitation spectrum suggests that energy transfer from the $^4I_{13/2}$ level of Er^{3+} to the $^3H_4$ level of Tm^{3+} occurs through the following multipolar interactions:

$$Er^{4+}: {}^4I_{13/2} \rightarrow {}^4I_{15/2}, \quad Tm^{3+}: {}^3H_6 \rightarrow {}^3H_4 .$$

Nonradiative energy transfer from the $^4F_{9/2}$ level to the $^3F_2$ level of Tm^{3+} is also consistent with the observation of the $^4F_{9/2}$ band in the excitation spectrum of the Tm^{3+} $^3F_4 \rightarrow {}^3H_6$ emission band.

As mentioned earlier, Tm^{3+} acts to quench the green fluorescence of Er^{3+}. The up-conversion efficiencies for the green emission (Table VI) reveal this behavior.

The Tm^{3+} $^3H_5$ band appears in the excitation spectrum of the Er^{3+} $^4I_{13/2} \rightarrow {}^4I_{15/2}$ emission band for the glass A(I) [Fig. 3(d)], indicating energy transfer from the

TABLE VIII. Ω_t parameters for Tm^{3+} in various glasses. Numbers appearing before compounds in formulas represent mol % of constituent.

Glass	Ω_2 (10^{-20} cm^2)	Ω_4 (10^{-20} cm^3)	Ω_6 (10^{-20} cm^{-2})	Ref.
Borate	5.42	2.78	1.66	37
Phosphate	5.88	2.88	0.71	37
Germanate	3.22	1.25	0.65	37
$51.2ZrF_4$-$18.3BaF_2$-$5LaF_3$-$3.5AlF_3$-$19.5LiF$-$2.5TmF_3$	2.80	1.91	1.01	38
$19BaF_2$-$27ZnF_2$-$26YbF_3$-$27ThF_4$-$1TmF_3$	1.14	1.57	1.13	14
$30BaF_2$-$20ZnF_2$-$30InF_3$-$8YF_3$-$10ThF_4$-$2TmF_3$	2.02	1.56	1.10	This work

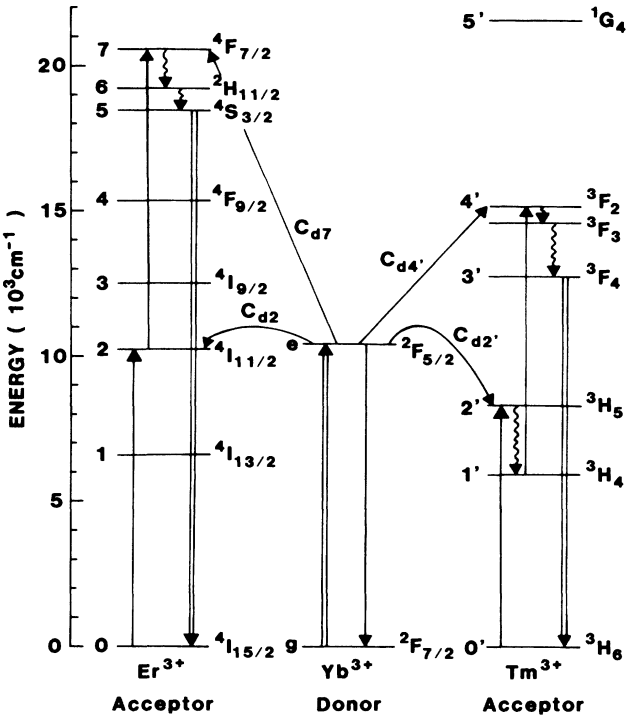

FIG. 7. Models for up-conversion in Yb^{3+}-Er^{3+} and Yb^{3+}-Tm^{3+} systems. Energy levels and transitions of the Er^{3+} and Tm^{3+} ions which are not considered important in the up-conversion process have been omitted.

$^3H_4$ level of Tm^{3+} to the $^4I_{13/2}$ level of Er^{3+}. The $^3F_3$ band of Tm^{3+} is also evident in the excitation spectrum, which suggests energy transfer from the $^3F_4$ level of Tm^{3+}. When a Tm^{3+} ion is excited to the $^3F_2$ or $^3F_3$ levels it decays rapidly to the $^4F_4$ emitting level by multiphonon relaxation. The transition from $^3F_4$ to $^3H_4$ results in cross relaxation to the transition of $^4I_{15/2} \rightarrow {}^4I_{13/2}$. This energy transfer mechanism is consistent with the excitation spectrum of the Er^{3+} $^4I_{13/2} \rightarrow {}^4I_{15/2}$ emission band for glass B, containing 4 mol% ErF_3 and 0.1 mol% TmF_3 [Fig. 4(b)]. Energy transfer from the $^3F_4$ level of Tm^{3+} to the $^4I_{9/2}$ level of Er^{3+} can also occur. However, the excitation spectra of Er^{3+} $^4I_{11/2} \rightarrow {}^4I_{15/2}$ emission show that there is no difference between the glasses B and C. This suggests that energy transfer from the $^3F_4$ level of Tm^{3+} to the $^4I_{9/2}$ level of Er^{3+} may not be possible.

For a Yb^{3+}-doped sample, the $^3H_4$ emission lifetime is reduced from 10 msec to a 4 msec when the sample is pumped with light corresponding to the Yb^{3+} absorption band. This indicates energy transfer from the $^3H_4$ level of Tm^{3+} to Er^{3+} ions. There are two possible steps. Energy transfer from the $^3H_4$ level of Tm^{3+} to the $^4I_{13/2}$ level of Er^{3+} may occur. A second possibility is that Yb^{3+} ions are excited from the ground level to the $^2F_{5/2}$ level and the excited Yb^{3+} ions transfer their energy to the Er^{3+} or Tm^{3+} ions, exciting them to the $^4I_{11/2}$ and $^3H_5$ levels, respectively. The Tm^{3+} $^3H_5$ level relaxes to the metastable state $^3H_4$ by a multiphonon decay and the $^4F_{9/2}$ level is then excited from the populated $^4I_{11/2}$ level by energy transfer from Tm^{3+}: $^3H_4 \rightarrow {}^3H_6$ to Er^{3+}: $^4I_{11/2} \rightarrow {}^4F_{9/2}$. This transfer is particularly important because it controls the $^4F_{9/2}$ up-conversion efficiency. This can explain why the quenching effect of Tm^{3+} on the red ($^4F_{9/2}$) emission is weaker than that for the green ($^4S_{3/2}$) emission. The quenching of the up-conversion process occurs at the lower excited levels. Direct excitation of the $^4S_{3/2}$ Er^{3+} level or the $^1G_4$ Tm^{3+} level results in normal emission from these levels. This has important implications for up-conversion lasers and infrared detection systems.

C. Energy transfer analysis

Materials containing Yb^{3+}-Er^{3+} or Yb^{3+}-Tm^{3+} ion combinations can efficiently convert 1.0-μm infrared light to visible light or near-infrared light.[1-4,13-15,18] There are several multiphoton mechanisms responsible for the up-conversion.[1,2] The most efficient mechanism is the absorption of pump photons by more than one ion with subsequent energy transfer to one emitting ion.[1,2] Since energy transfer plays such an important role in laser and up-conversion processes, it is helpful to try to predict the most efficient impurity types and concentrations. A simple rate equation model can be used to describe up-conversion and energy transfer between donor and acceptor ions. We will consider two cases. One for materials containing Yb^{3+} ions and one for materials with no Yb^{3+}.

In case I, the Er^{3+}-Yb^{3+}-Tm^{3+} system is considered. Figure 7 illustrates up-conversion for the Er^{3+}, Yb^{3+}, and Tm^{3+} system. The notation on the right-hand side of each manifold represents the level. The labels used in the rate equations below are shown on the left-hand side. When the Yb^{3+} $^2F_{5/2}$ level is pumped, the appropriate steady-state rate equations are

$$\dot{n}_e^d = \sigma_2^d \phi_2 n_g^d - C_{d2} n_e^d n_0 + C_{2d} n_g^d n_2 - C_{d2'} n_e^d n_{0'} + C_{2'd} n_g^d n_{2'} - \tau_d^{-1} n_e^d = 0 , \quad (2)$$

$$\dot{n}_1 = W_{21} n_2 - C_{11'} n_1 n_{0'} + C_{1'1} n_{1'} n_0 - \tau_1^{-1} n_1 = 0 , \quad (3)$$

$$\dot{n}_2 = C_{d2} n_e^d n_0 - C_{d2} n_g^d n_2 - \tau_2^{-1} n_2 - C_{22'} n_2 n_{0'} - W_{21} n_2 = 0 , \quad (4)$$

$$\dot{n}_{1'} = W_{2'1'} n_{2'} + C_{11'} n_1 n_{0'} - C_{1'1} n_{1'} n_0 - \tau_{1'}^{-1} n_{1'} = 0 , \quad (5)$$

$$\dot{n}_{2'} = C_{d2'} n_e^d n_{0'} + C_{22'} n_2 n_{0'} - W_{2'1'} n_{2'} = 0 . \quad (6)$$

Several approximations have been made in obtaining these equations. Stimulated emission terms have been ignored, transitions from the $^4S_{3/2}$ level to the $^4I_{11/2}$ level and from the $^3F_4$ level to the $^3H_5$ level are not considered, back transfer from $^3H_5$ level to the $^2F_{5/2}$ level or the $^4I_{11/2}$ level is neglected, and the transfer to and from the $^4F_{7/2}$ level or the $^3F_2$ level is normally insignificant compared with the other processes affecting the $^2F_{5/2}$, $^4I_{11/2}$, and $^3H_5$ levels. The levels of the donor ion are denoted by a superscript d. A subscript g is used if the ground-state level is involved or e if excited-state level is involved. The W_{ij} terms represent the transition rates

between levels i and j. The C_{ij} terms are the transfer rates between levels i and j. The lifetime of level i in the absence of ion-ion transfer is denoted by τ_i. σ_2^d is the absorption cross section of donor ions and ϕ_2 is the incident pumping flux. If the pumping intensity is sufficiently weak that the ground states are not depopulated, $n_g^d = N_Y$, $n_0 = N_E$, and $n_{0'} = N_T$, where N_Y, N_E, and N_T are the concentrations of Yb^{3+}, Er^{3+}, and Tm^{3+} ions, respectively.

The fluorescence intensity from level i to the ground state is defined as

$$I_i = \hbar\omega_{i0} W_{i0} n_i \ . \tag{7}$$

The important experimental parameters for this case in A(II) glass at 15 K are $I_1/I_d = 0.002$, $I_2/I_d = 0.018$, and $I_{1'}/I_d = 0.053$. The others are $\sigma_2^d = 2.5\times10^{-20}$ cm^2, $\phi_2 = 1.97\times10^{17}$ cm^{-2}sec^{-1}, $\tau_d^{-1} = 500$ sec^{-1}, $\tau_1^{-1} = 98$ sec^{-1}, $\tau_2^{-1} = 98$ sec^{-1}, $\tau_{1'}^{-1} = 94$ sec^{-1}, $W_{2'1'} = 10^4$ sec^{-1}, $W_{21} = 10$ sec^{-1}, $N_E = 1.88\times10^{20}$ cm^{-3}, $N_Y = 1.88\times10^{21}$ cm^{-3}, and $N_T = 1.88\times10^{19}$ cm^{-3}. From Eq. (7) and the measured intensity ratios we find $n_e^d/n_1 = 63.3$, $n_e^d/n_{1'} = 1.93$, $n_e^d/n_2 = 11.1$, $n_1/n_2 = 0.176$, $n_{1'}/n_2 = 5.75$, and $n_1/n_{1'} = 0.0306$. In this discussion we consider only the experimental results and the theoretical calculations valid for 15 K. Judd-Ofelt analysis is most valid when there is an equal population of all M_j levels. This occurs at high temperature. However, in our complicated system energy transfer dominates at high temperature and the most applicable values are obtained at 15 K.

It is possible to excite the $^4I_{13/2}$ level directly and obtain valuable information. The appropriate steady-state rate equations for excitation in this level are

$$\dot{n}_1 = \sigma_1^d \phi_1 N_E - C_{11'} n_1 N_T + C_{1'1} n_{1'} N_E - \tau_1^{-1} n_1 = 0 \ , \tag{8}$$

$$\dot{n}_{1'} = C_{11'} n_1 N_T - C_{1'1} n_{1'} N_E - \tau_{1'}^{-1} n_{1'} = 0 \ . \tag{9}$$

In this case, $\sigma_1^d = 5\times10^{-21}$ cm^2, $\phi_1 = 2.21\times10^{16}$ cm^{-2}sec^{-1}, $I_{1'}/I_1 = 0.395$, and the other parameters are the same as noted previously. From Eq. (7) and the intensity ratio we find $n_{1'}/n_1 = 0.492$.

The solution of equations, Eqs. (2)–(6) as well as Eqs. (8) and (9), leads to the following values:

$$C_{11'} N_T = 48 \text{ sec}^{-1} \ , \tag{10}$$

$$C_{1'1} N_E = 2.7 \text{ sec}^{-1} \ , \tag{11}$$

$$C_{22'} N_T \approx 0 \text{ sec}^{-1} \ , \tag{12}$$

$$C_{d2'} N_T = 49 \text{ sec}^{-1} \ , \tag{13}$$

$$C_{2d} N_Y = 11.1 C_{d2} N_E - 108 \text{ sec}^{-1} \ . \tag{14}$$

The concentrations of the excited-state levels for excitation in the $^2F_{5/2}$ level are $n_e^d = 1.66\times10^{16}$ cm^{-3}, $n_1 = 2.62\times10^{14}$ cm^{-3}, $n_2 = 1.5\times10^{15}$ cm^{-3}, $n_{1'} = 8.6\times10^{15}$ cm^{-3}, and $n_{2'} = 8.2\times10^{13}$ cm^{-3}.

The up-conversion mechanism for glass containing only Er^{3+} and Tm^{3+} (case II) is depicted in Fig. 8. The appropriate steady-state rate equations for excitation in the Er^{3+} $^4I_{11/2}$ level are

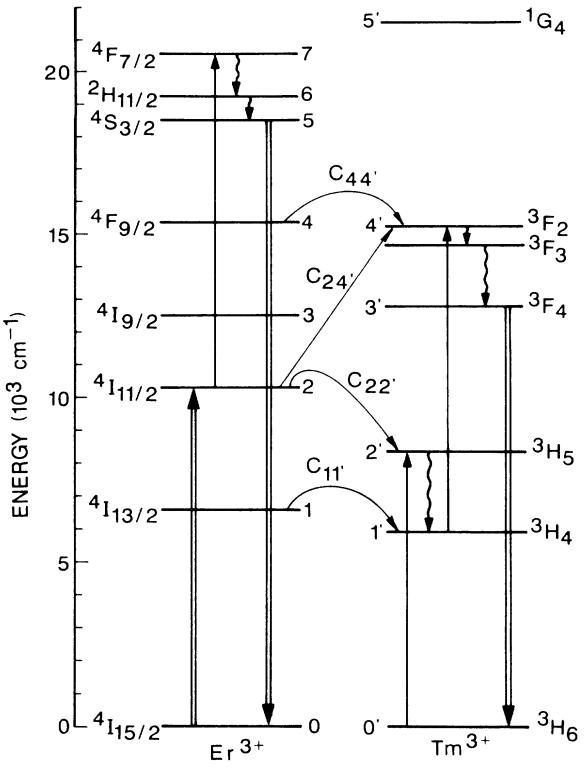

FIG. 8. Models for up-conversion in Er^{3+}-Tm^{3+} system. Energy levels and transitions of the Er^{3+} and Tm^{3+} ions which are not considered important in the up-conversion process have been omitted.

$$\dot{n}_1 = W_{21} n_2 - C_{11'} n_1 N_T + C_{1'1} n_{1'} N_E - \tau_1^{-1} n_1 = 0 \ , \tag{15}$$

$$\dot{n}_2 = \sigma_{II}^d \phi_{II} N_E - C_{22'} n_2 N_T - \tau_2^{-1} n_2 - W_{21} n_2 = 0 \ , \tag{16}$$

$$\dot{n}_{1'} = C_{11'} n_1 N_T - C_{1'1} n_{1'} N_E + W_{2'1'} n_{2'} - \tau_{1'}^{-1} n_1 = 0 \ , \tag{17}$$

$$\dot{n}_{2'} = C_{22'} n_2 N_T - W_{2'1'} n_{2'} = 0 \ . \tag{18}$$

The same approximations as described in case I have been used to obtain these equations. The relevant experimental parameters for glass B are $I_1/I_2 = 0.0166$, $I_{1'}/I_2 = 0.051$, $I_{1'}/I_1 = 3.07$, $\sigma_{II}^d = 4\times10^{-21}$ cm^2, $\phi_{II} = 1.69\times10^{17}$ cm^{-2}sec^{-1}, $\tau_1^{-1} = 98$ sec^{-1}, $\tau_2^{-1} = 98$ sec^{-1}, $\tau_{1'}^{-1} = 94$ sec^{-1}, $W_{2'1'} = 10^4$ sec^{-1}, $W_{21} = 10$ sec^{-1}, $N_E = 7.52\times10^{20}$ cm^{-3}, and $N_T = 1.88\times10^{19}$ cm^{-3}. We find $n_1/n_{1'} = 0.262$, $n_1/n_2 = 0.0261$, and $n_{1'}/n_2 = 0.1$.

The steady-state rate equations for excitation in the $^4I_{13/2}$ level, are

$$\dot{n}_1 = \sigma_I^d \phi_I N_E - C_{11'} n_1 N_T + C_{1'1} n_{1'} N_E - \tau_1^{-1} n_1 = 0 \ , \tag{19}$$

$$\dot{n}_{1'} = C_{11'} n_1 N_T - C_{1'1} n_{1'} N_E - \tau_{1'}^{-1} n_{1'} = 0 \ . \tag{20}$$

In this case, $\sigma_I^d = 5\times10^{-21}$ cm^2, $\phi_I = 2.21\times10^{16}$ cm^{-2}sec^{-1}, and $I_1/I_{1'} = 0.41$. The other parameters are the same for excitation in the $^4I_{11/2}$ level and $n_1/n_{1'} = 0.33$.

The solution of these equations leads to the result

$$C_{11'}N_T = 290 \text{ sec}^{-1} , \quad (21)$$

$$C_{1'1}N_E = 1.7 \text{ sec}^{-1} , \quad (22)$$

$$C_{22'}N_T = 2 \text{ sec}^{-1} , \quad (23)$$

and the concentrations of the excited-state levels for excitation in the $^4I_{11/2}$ level are $n_1 = 1.2 \times 10^{14}$ cm^{-3}, $n_2 = 4.62 \times 10^{15}$ cm^{-3}, $n_{1'} = 4.62 \times 10^{14}$ cm^{-3}, and $n_{2'} = 9 \times 10^{11}$ cm^{-3}.

It is noted that the energy transfer rates of $C_{22'}N_T$ are much smaller than those of $C_{11'}N_T$ in both Yb^{3+}-doped and non-Yb^{3+}-doped materials. This indicates that energy transfer between Er^{3+} and Tm^{3+} ions occurs primarily at the lowest excited-state levels. This observation is helpful in understanding the work of van der Ziel *et al.*[16] They used 1.5-μm infrared excitation of $Y_{1-x-y}Er_xTm_yF_3$ crystals and found that the green $^4S_{3/2}$ emission was quenched in samples containing between 0.1% and 2% of the Tm^{3+} ions. When they increased the Tm^{3+} content to more than 3% a nearly complete quenching of all visible Er^{3+} emission occurred. In all cases they found no Tm^{3+} emission.[16] Our results suggest that when a sample is pumped with 1.5-μm infrared radiation, most of the Er^{3+} energy transfer should occur from the Er^{3+} $^4I_{13/2}$ level to the Tm^{3+} $^3H_4$ level due to the high energy transfer rate. Thus the visible Er^{3+} emission would be quenched. Moreover, although no Tm^{3+} emission was observed by van der Ziel *et al.*,[16] we believe that in most samples strong Tm^{3+} infrared emission corresponding to the transition of $^3H_4 \rightarrow {}^3H_6$ should be observed. In order to understand the up-conversion process a thorough evaluation of energy transfer must be made. The fact that $C_{1'1}N_E \ll C_{11'}N_T$ suggests that the back transfer efficiency of energy from the Er^{3+} $^4I_{13/2}$ level to the Tm^{3+} $^3H_4$ level is negligible as compared with forward transfer at 15 K. A comparison of the energy transfer rates $C_{11'}N_T$ between glass A(II), containing 1 mol% ErF_3 and 0.1 mol% TmF_3, and glass B, containing 4 mol% ErF_3 and 0.1 mol% TmF_3, yields a ratio of 6. If the Er^{3+} and Tm^{3+} ions are randomly distributed inside these glasses, the ratio of the concentration of Er^{3+}-Tm^{3+} pairs for these two glasses would be 4. This slight discrepancy is likely due to Er^{3+}-Er^{3+} energy transfer since energy transfer between Er^{3+} ions in the glass containing 4 mol% ErF_3 is more efficient than that for the glass containing 1 mol% ErF_3.

D. Cross-section calculations

Laser action at 549.6 nm has been achieved in the $YAlO_3$:Er^{3+} crystal for the $^4S_{3/2} \rightarrow {}^4I_{15/2}$ transition.[7] It is interesting to calculate the stimulated emission cross section for this transition in glass A(I) and compare it with that obtained for Zr-based fluoride glass.[36] The stimulated emission cross section can be expressed as

$$\sigma(\lambda_p) = \frac{\lambda_p^4}{8\pi c n^2 \Delta\lambda_{\text{eff}}} A(aJ, bJ') , \quad (24)$$

where λ_p is the peak fluorescence wavelength of the emission band $\Delta\lambda_{\text{eff}}$ is the effective fluorescence bandwidth determined by dividing the integrated fluorescence line shape by the intensity at λ_p. In our case $\lambda_p = 548$ nm, $n = 1.518$, $\Delta\lambda_{\text{eff}} = 8.67$ nm and A ($^4S_{3/2} \rightarrow {}^4I_{15/2}$) $= 696.7$ sec^{-1}, we obtain $\sigma(\lambda_p) = 0.42 \times 10^{-20}$ cm^2, which is about 60% of the value given for Zr-based fluoride glass.

We have some concern about the value for this "effective" linewidth, since these lines are inhomogeneously broadened in glasses. Weber[39,40] has discussed this in detail and we use a value consistent with other published values for comparison purposes.

Lasing emission at about 3 μm, corresponding to the $^4I_{11/2} \rightarrow {}^4I_{13/2}$ transition of Er^{3+} in CaF_2 (Ref. 6) and in $YAlO_3$ (Ref. 41) was recently reported. The corresponding stimulated emission cross section for this transition in glass B is 1.64×10^{-20} cm^2. In addition, the stimulated emission cross section for Tm^{3+} $^1D_2 \rightarrow {}^3H_4$ in glass A(I) is 1.68×10^{-20} cm^2, which is also about 60% of the value obtained for Zr-based fluoride glass.[38]

V. CONCLUSIONS

The Judd-Ofelt analysis and the up-conversion studies for Er^{3+} and Tm^{3+} ions in both Yb^{3+}-doped and non-Yb^{3+}-doped BaF_2-ThF_4 fluoride glasses have established the following points.

(i) The intensity parameters obtained from the Judd-Ofelt analysis suggest that BaF_2-ThF_4 fluoride glass is highly ionic.

(ii) The addition of Tm^{3+} preferentially quenches the up-conversion efficiency of $^4S_{3/2}$ green emission. The decrease in emission amounts to a factor of about 50 for the concentration of 0.5 mol% TmF_3 at 300 K. The quenching effect is due to energy transfer between Er^{3+} and Tm^{3+}.

(iii) Rate equations when used in conjunction with the appropriate optical data lead to an understanding of the up-conversion process and can be used to evaluate the absolute values of the energy transfer rates as well as the electron populations at the lower excited-state levels of Er^{3+} and Tm^{3+} ions. This has important implications for the up-conversion laser or the infrared laser devices. For example, lasing of the $^4I_{11/2} \rightarrow {}^4I_{13/2}$ transition may be best achieved in BaF_2-ThF_4 fluoride glass co-doped with the appropriate concentrations in Er^{3+} and Tm^{3+} ions. An appropriate concentration of Tm^{3+} ions would enhance the energy transfer rate from the Er^{3+} $^4I_{13/2}$ level to the Tm^{3+} $^3H_4$ level. This would reduce the effective lifetime of the $^4I_{13/2}$ transition and enhance the population inversion between $^4I_{11/2}$ and $^4I_{13/2}$.

ACKNOWLEDGMENTS

The authors are very grateful to Dr. W. T. Carnall from the Chemistry Division, Argonne National Laboratory, for providing the reduced matrix elements for Tm^{3+} in LaF_3. This research was sponsored by the U.S. Department of the Air Force under Contract No. F-19628-86-C-0138.

[1]F. E. Auzel, Proc. IEEE **61**, 758 (1973); Phys. Rev. B **13**, 2809 (1976); *Upconversion by Energy Transfer* (World Science, Singapore, 1985).
[2]J. C. Wright, Topics Appl. Phys. **15**, 239 (1976).
[3]A. A. Bergh and P. J. Dean, *Light-Emitting Diodes* (Clarendon, Oxford, 1976), pp. 343–383.
[4]L. F. Johnson and H. J. Guggenheim, Appl. Phys. Lett. **19**, 44 (1971).
[5]G. T. Basiev, E. V. Zharikov, V. I. Zhekov, T. M. Murina, V. V. Osiko, A. M. Prokhorov, B. P. Starikov, M. I. Timoshechkin, and I. A. Scherbakov, Sov. J. Quantum Electron. **6**, 796 (1976).
[6]S. A. Pollack, D. B. Chang, and N. L. Moise, J. Appl. Phys. **60**, 4077 (1986); Appl. Phys. Lett. **49**, 1578 (1986).
[7]A. J. Silversmith, W. Lenth, and R. M. Macfarlane, Appl. Phys. Lett. **51**, 1977 (1987).
[8]G. D. Gilliland, R. C. Powell, and L. Esterowitz, Phys. Rev. B (to be published).
[9]M. G. Drexhage, in *Treatise on Materials Science and Technology,* edited by M. Tomozawa and R. H. Doremus (Academic, New York, 1985), Vol. 26, pp. 151–243.
[10]P. W. France, S. F. Carter, M. W. Moore, and C. R. Day, Br. Telecommun. Technol. J. **5**, 28 (1987).
[11]W. A. Sibley, D. C. Yeh, Y. Suzuki, G. J. Quarles, and R. C. Powell, in *Defect in Glasses,* edited by F. L. Galeener, D. L. Griscom, and M. J. Weber (Materials Research Society, Pittsburgh, 1986), p. 239.
[12]P. W. France and M. C. Brierley, Electron. Lett. **23**, 815 (1987).
[13]D. C. Yeh, W. A. Sibley, M. Suscavage, and M. G. Drexhage, J. Appl. Phys. **62**, 266 (1987).
[14]D. C. Yeh, W. A. Sibley, and M. J. Suscavage, J. Appl. Phys. **63**, 4644 (1988).
[15]R. S. Quimby, M. G. Drexhage, and M. J. Suscavage, Electron. Lett. **23**, 32 (1987).
[16]J. P. van der Ziel, L. G. Van Uitert, W. H. Grodkiewicz, and R. M. Mikulyak, J. Appl. Phys. **60**, 4262 (1986).
[17]J. P. Jouart, J. Lumin. **21**, 153 (1980).
[18]L. F. Johnson, H. J. Guggenheim, T. C. Rich, and F. W. Ostermayer, J. Appl. Phys. **43**, 1125 (1972).
[19]B. R. Judd, Phys. Rev. **127**, 750 (1962).
[20]G. S. Ofelt, J. Chem. Phys. **37**, 511 (1962).
[21]W. F. Krupke, Phys. Rev. **145**, 325 (1966).
[22]M. J. Weber, Phys. Rev. **157**, 262 (1967).
[23]W. T. Carnall, P. R. Fields, and K. Rajank, J. Chem. Phys. **49**, 4424 (1968).
[24]M. J. Weber, Phys. Rev. B **8**, 54 (1973).
[25]R. Reisfeld and Y. Eckstein, J. Non-Cryst. Solids **15**, 125 (1974).
[26]M. D. Shinn, W. A. Sibley, M. G. Drexhage, and R. N. Brown, Phys. Rev. B **27**, 6635 (1983).
[27]K. Tanimura, M. D. Shinn, W. A. Sibley, M. G. Drexhage, and R. M. Brown, Phys. Rev. B **30**, 2429 (1984).
[28]J. Lucas, H. Slim, and G. Fonteneau, J. Non-Cryst. Solids **44**, 31 (1981).
[29]M. G. Drexhage, O. H. El-Bayoumi, C. T. Moynihan, A. J. Bruce, K.-H. Chung, D. L. Gavin, and T. J. Loretz, J. Am. Ceram. Soc. **65**, C-168 (1982).
[30]S. Mitachi, G. Fonteneau, P. S. Christensen, and J. Lucas, J. Non-Cryst. Solids **92**, 313 (1987).
[31]W. T. Carnall, Hannah Crosswhite, and H. M. Crosswhite, *Energy Level Structure and Transition Probabilities of the Trivalent Lanthanides in* LaF_3 (John Hopkins University, Baltimore, 1977).
[32]C. K. Jorgensen and R. Reisfeld, J. Less-Common Met. **93**, 107 (1983).
[33]R. Reisfeld, J. Electrochem. Soc. **131**, 1360 (1984).
[34]F. Auzel, Ann. Telecommun. **24**, 199 (1969).
[35]R. Reisfeld and Y. Eckstein, Solid State Commun. **13**, 265 (1973).
[36]R. Reisfeld, G. Katz, C. Jacoboni, R. De Pape, M. G. Drexhage, R. N. Brown, and C. K. Jorgensen, J. Solid State Chem. **48**, 323 (1983).
[37]R. Reisefeld And Y. Eckstein, J. Chem. Phys. **63**, 4001 (1975).
[38]J. Sanz, R. Cases, and R. Alcala, J. Non-Cryst. Solids **93**, 377 (1987).
[39]G. J. Linford, R. A. Saroyan, J. B. Trenholme, and M. J. Weber, IEEE J. Quantum Electron. **QE-15**, 510 (1979).
[40]M. J. Weber, Ceram. Bull. **64**, 1439 (1985).
[41]M. Stalder and W. Luthy, J. Appl. Phys. **62**, 3570 (1987).